

## Junocam: Juno's Outreach Camera

C.J. Hansen · M.A. Caplinger · A. Ingersoll ·  
M.A. Ravine · E. Jensen · S. Bolton · G. Orton

Received: 4 September 2013 / Accepted: 23 July 2014  
© The Author(s) 2014. This article is published with open access at Springerlink.com

**Abstract** Junocam is a wide-angle camera designed to capture the unique polar perspective of Jupiter offered by Juno's polar orbit. Junocam's four-color images include the best spatial resolution ever acquired of Jupiter's cloudtops. Junocam will look for convective clouds and lightning in thunderstorms and derive the heights of the clouds. Junocam will support Juno's radiometer experiment by identifying any unusual atmospheric conditions such as hotspots. Junocam is on the spacecraft explicitly to reach out to the public and share the excitement of space exploration. The public is an essential part of our virtual team: amateur astronomers will supply ground-based images for use in planning, the public will weigh in on which images to acquire, and the amateur image processing community will help process the data.

**Keywords** Juno · Jupiter · Jupiter's poles · Jupiter's atmosphere · images of Jupiter

---

C.J. Hansen  
Planetary Science Institute, Tucson, AZ, USA

M.A. Caplinger · M.A. Ravine · E. Jensen  
Malin Space Science Systems, San Diego, CA, USA

A. Ingersoll  
California Institute of Technology, Pasadena, CA, USA

S. Bolton  
Southwest Research Institute, San Antonio, TX, USA

G. Orton  
Jet Propulsion Laboratory, California Institute of Technology, Pasadena, CA, USA

C.J. Hansen (✉)  
389 N. Industrial Rd., Suite 5, St. George, UT 84770, USA  
e-mail: [cjhansen@psi.edu](mailto:cjhansen@psi.edu)

## 1 Introduction

The scientific themes of the Juno mission are to study the interior, atmosphere, and magnetosphere of Jupiter (Bolton et al., this issue). The spacecraft has been highly optimized for the operation of its seven science instruments, leading to a solar-powered, sun-pointing, spinning design. Such a platform presents challenges for imaging, both from motion blur and pointing geometry. But it was appreciated that visible imaging is an important component of public engagement for any mission. So a visible camera, Junocam, was included primarily for education and public outreach (EPO), funded from the mission's EPO budget and given a fairly constrained allocation of spacecraft mass resources.

Despite the challenges, Juno's polar orbit offers a unique vantage point for imaging Jupiter compared to other missions that have orbited or flown by Jupiter. The orbital inclination is high, and the closest point in the orbit, perijove, is near the equator. The orbit plane is nearly perpendicular to the Sun-Jupiter line, so the spacecraft is generally flying along the terminator. The orbit enables observation of the poles at low emission angles, and features close approaches to Jupiter—about 5000 km above the cloud tops at perijove. This allows almost an order of magnitude improvement in resolution compared with Galileo's best, which is in the range 20–25 km (Little et al. 1999). No imaging was obtained during Galileo's end-of-mission impact into Jupiter.

The science and EPO objectives evolved from trade studies balancing the unique imaging opportunities arising from the Juno orbit with the constraints of cost and spacecraft resources (mass, volume and power) available for an EPO camera. Observing the pole is one such opportunity, both for EPO and science, and it leads to the requirement of imaging the entire polar region in three colors (red, green and blue) as the spacecraft passes over the poles  $\pm 1$  h from closest approach. This in turn leads to a field of view requirement of about 60 degrees. Another opportunity is studying the equatorial region at ten times higher spatial resolution than that of Voyager, Galileo, and Cassini. It leads to a resolution requirement of 3 km/pixel at perijove, when the spacecraft is near the equator, and 50 km/pixel when the spacecraft is over the pole.

The third opportunity is to serve as the “eyes” in visible and near-infrared light for other remote sensing instruments on Juno. These include the microwave radiometer (MWR), the ultraviolet imaging spectrograph (UVS), and the Jovian infrared auroral mapper (JIRAM). Since clouds are both signal and noise for these instruments, the ability to image clouds becomes an additional requirement for Junocam. This is addressed by having a filter at 889 nm, which is an absorption band of methane, a well-mixed gas in Jupiter's atmosphere. High clouds and hazes stand out in 889 nm images, since they reflect more sunlight than the absorbing gas around them. A single methane filter is not a comprehensive cloud detector, but it is the optimal choice given severe constraints of cost, mass, camera sensitivity, and compatibility with the basic camera design.

To optimize the camera design within constrained resources, the camera electronics design is based on that developed earlier for the Mars Science Laboratory (MSL) mission (Edgett et al. 2012). The flexibility inherent in that design allowed the addition of multiband “pushframe” imaging and time-delayed integration (TDI), described in Sect. 3. These enhancements give adequate signal to noise ratio (SNR) in the images despite the spin of the spacecraft. The radiation environment for Juno, while avoiding the worst areas of the jovian radiation belts, is still many times harsher than that of the MSL mission. Substantial extra shielding mass was added to both the optics and electronics and some revision was made to selected parts. While Junocam is only required and qualified to survive for the first three months of the mission (through orbit 8), we expect the degradation of the instrument to be graceful.

**Fig. 1** The Junocam camera head and its associated electronics (Junocam Digital Electronics Assembly: JDEA) are shown. The camera head is 7.5" tall



**Fig. 2** The Junocam camera head is mounted to the side of the spacecraft, with its boresight perpendicular to the spacecraft rotation axis



The remainder of this introduction is a brief overview of the camera and its field of view during the hours around closest approach. Section 2 gives the expected science return. Section 3 gives the detailed instrument description. Section 4 describes the calibration results. Section 5 describes operations and commanding, and Section 6 gives the outreach plans.

Junocam is shown in Fig. 1. It was built and is being operated by Malin Space Science Systems (MSSS) in San Diego, California. Figure 2 shows a close-up image of Junocam mounted on the Juno spacecraft. The camera's boresight is perpendicular to the spacecraft spin axis. The detector is an array, with the rows of pixels aligned parallel to the spacecraft's rotation axis, that sweeps across the target as the spacecraft spins. The width of an image is set by the  $58^\circ$  angular width of the detector array. The length of an image is not really constrained—it could cover a full  $360^\circ$  of spacecraft rotation, but a typical image of Jupiter will extend along the scan direction from one limb to the other.

A simulated view of the pole of Jupiter as seen by Junocam is shown in Fig. 3. The image footprint is swept out by Junocam's detector array during one 30 s rotation of the spacecraft, which nominally spins at 2 rpm. The red-green-blue data is collected in one 30 s rotation, followed by the methane image on the subsequent rotation, resulting in acquisition of one 4-

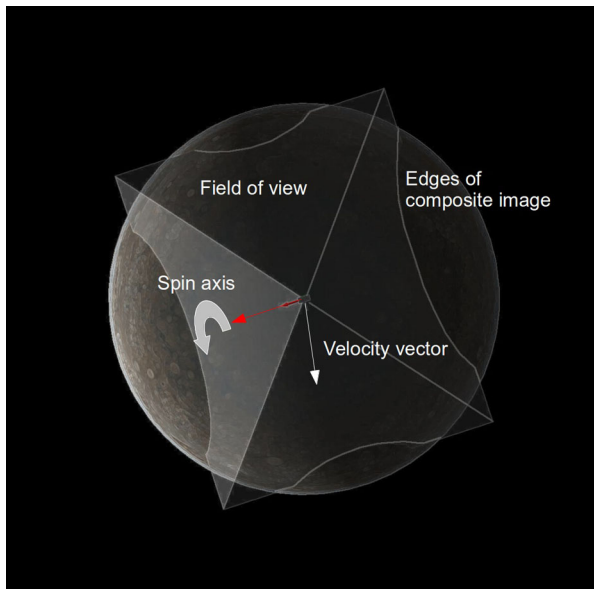


**Fig. 3** This is a simulated view of the north pole of Jupiter as seen by Junocam  $\sim 1$  h before perijove on Orbit 16. The semitransparent pyramid represents the portion of the instrument's  $58 \times 360$  degree total field of view that contains the planet. The spacecraft rotates counterclockwise about its spin axis, which is shown by the *red arrow*. The footprint has a quasi-rectangular shape whose short dimension is defined either by the angular width of the detector array (extent off the body shown in this figure) or by the horizon (as in the middle of this illustration). The long dimension of the image is defined by the contact points as the array is swept from the northern limb to the southern limb of the planet. The apex of the pyramid is at the spacecraft, and the sun-facing side is shown brighter than the others. The velocity vector shows the direction (north to south) the spacecraft is traveling in its orbit. Potential image smear is dominated by the spacecraft rotation, not its translational motion, and has been mitigated in the camera design.

color image per minute. As these spin-scan images are being taken the spacecraft is moving from north to south in its orbit. Figure 4 shows how the perspective changes during the 2 h of one pass through perijove (PJ).

## 2 Expected Science Return

Junocam takes advantage of Juno's unique polar orbit, its extremely low-altitude perijove, and its complementary suite of instruments that probe the interior and atmosphere. The orbit enables one to study the atmospheric dynamics, the clouds, and the aurora right up to the pole, which no spacecraft has ever done before. The orbit also enables one to study the equatorial clouds and winds "up close," with a spatial scale of 3 km per pixel at perijove. Finally, Junocam provides "eyes" in visible light for three other instruments, the microwave radiometer (MWR), which peers through the clouds down to 100 bar levels (Janssen et al. 2014), the ultraviolet imaging spectrograph (UVS), which studies UV auroral emissions in the polar magnetosphere (Gladstone et al. 2014), and the Jovian infrared auroral mapper (JIRAM), which studies IR auroral emissions and the IR emissions emanating from the clouds at all latitudes (Adriani et al. 2014).

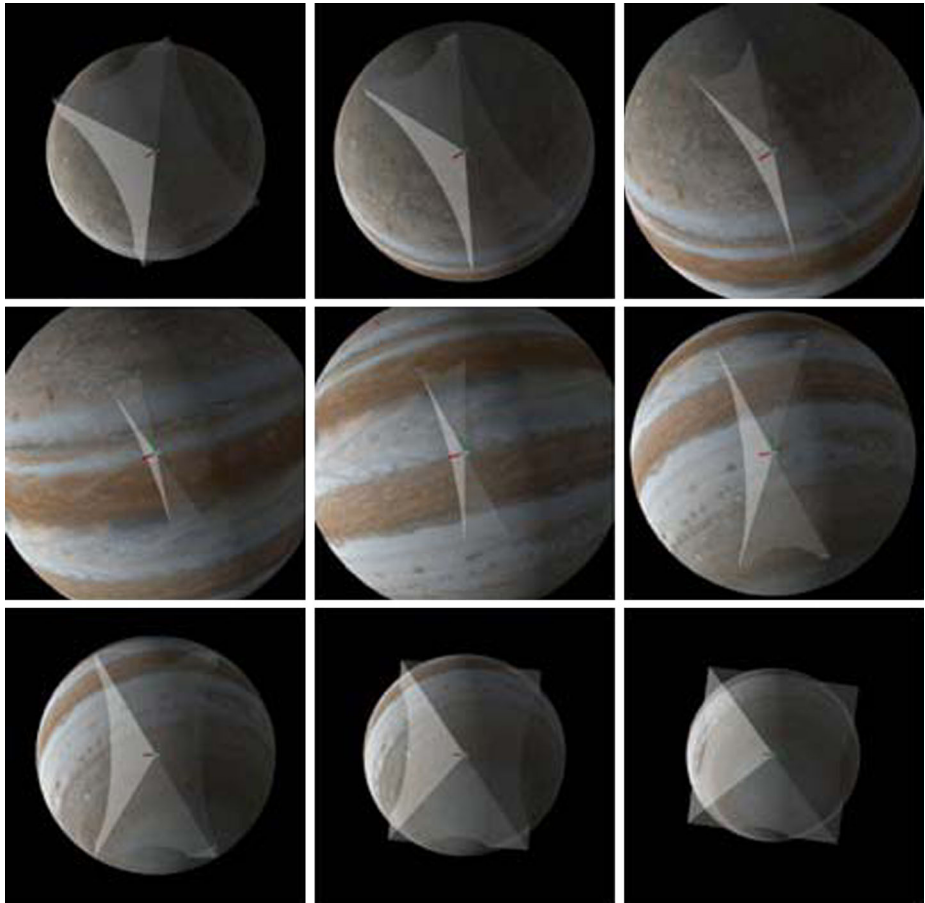


**Fig. 4** A series of simulated views from  $-1$  h to  $+1$  h for Orbit 10 shows the rapid changes in perspective of the Junocam images as Juno passes through perijove. Because the optics were sized for the polar views the footprint is  $\sim$  square when the spacecraft is  $\pm 1$  h from perijove. When it is closer the field of view is constrained in width to  $58^\circ$  but in length by the angular extent Jupiter subtends as seen from the spacecraft as it rotates, resulting in a long narrow image. The curved base of the pyramid follows the visible limb of the planet as seen from Juno; this visualization method is intended to show the areal coverage of each Junocam image, which varies with orbital altitude

Junocam science objectives are:

- (a) Investigate the nature and scale of meteorological phenomena at the poles, filling in the lack of coverage by Voyager, Galileo, and Cassini. Study the circumpolar waves detected by those earlier spacecraft.
- (b) Investigate atmospheric phenomena at scales ten times finer than those resolved by Voyager, Galileo, and Cassini.
- (c) Serve as the “eyes” for other instruments on the Juno spacecraft by imaging clouds—at the poles, at high altitudes, and at high resolution.

With its  $58^\circ$  field of view and the elliptical Juno orbit, Junocam exceeds the resolution of Cassini's imager at  $\sim -1$  h. At Juno perijove the spatial scale is  $\sim 3$  km/pixel, over an order of magnitude better than Cassini (Porco et al. 2003).

## 2.1 Jupiter

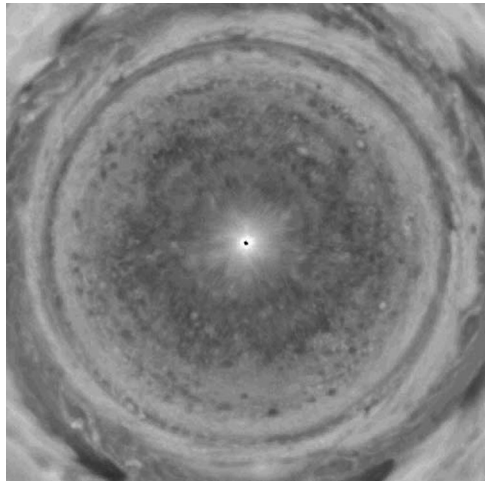
To understand Junocam's contributions to our knowledge of giant planets, it is good to review what we know and don't know about them. Jupiter and Saturn come closest to solar composition, but they seem to be enriched in elements heavier than hydrogen and helium by factors ranging from 2 to 10 (Niemann et al. 1998; Mahaffy et al. 2000; Atreya 2010). Despite this enrichment, the heavier elements contribute less than 1 % of the atoms in these planets' atmospheres and interiors. Oxygen, which is the third most abundant element on the Sun after hydrogen and helium, is a conundrum. It appears as water, but not in the right abundance. The Galileo probe went into a dry place, a so-called 5-micron hot spot, which is a giant hole in the clouds that allows 5-micron thermal emission from warmer, deeper levels to escape (Ortiz et al. 1998). It would be easy to blame water's poor showing on the meteorology of hot spots, but it would be better to find the water and to understand hot spot meteorology (Bjoraker et al. 1986; Roos-Serote et al. 2004).

Junocam can identify the hot spots and examine them at high spatial resolution (Vasavada et al. 1998). It can look for convective clouds and lightning (Gierasch et al. 2000); it can estimate cloud heights using stereo and methane band imaging, and it can help the JIRAM instrument as it measures temperatures and cloud optical thickness. It will be able to measure small-scale winds if they are large enough (Vasavada et al. 1998). Junocam can define the structure at cloud top level—the belts and zones and their dynamical structures—to correlate with the water and ammonia abundance that MWR is measuring deeper down. Since meteorology affected the water measurement by the Galileo probe, it is important to know the meteorology and how it might affect the water measurement by the Juno MWR.

Junocam's 3 km per pixel horizontal resolution near perijove is unprecedented. It will allow one to see individual features within thunderstorms. On Earth, thunderstorms are about as wide as they are tall, and range up to 15 km in both dimensions. Within each storm there are smaller-scale features. Juno will be able to see these small structures if they are present. One problem is that thunderstorms are relatively rare on Jupiter. The Galileo imaging system detected 26 lightning storms, typically 1000 km in diameter, on the night side of Jupiter (Little et al. 1999), implying that the typical distance between storms is about 10,000 km. In contrast, Earth has  $\sim 2000$  thunderstorm spread over the planet at any one time (Uman 1987), implying that the typical distance between them is  $\sim 500$  km. We are discussing thunderstorms because they have small-scale structures, but it is possible that other meteorological features have small-scale structures that Junocam will discover at 3 km per pixel resolution.

Junocam measures the height of the clouds in three ways. One is by stereo imaging; another is from cloud shadows, and the third is by methane band imaging. Most of the time the spacecraft's spin axis and orbital axis are both pointed toward Earth. As the spacecraft spins, the field of view of the instruments, including Junocam, sweeps repeatedly along the path of the spacecraft on the clouds below. Junocam takes a 4-color image every 60 s, during which time the spacecraft moves along its path by  $\sim 3400$  km. At closest approach, a point on the planet seen at nadir ( $0^\circ$  emission angle) will be seen at least six other times—at emission angles of  $\pm 34^\circ$ ,  $\pm 54^\circ$ , and  $\pm 64^\circ$ , which offers excellent opportunities for measuring the relative heights of clouds. To measure the cloud height variations, they must be at least 3 km, since that is the pixel size at perijove. Such heights are likely, since the scale height in the mid troposphere is 20–25 km. The spacecraft is flying close to the terminator, so cloud shadows will project several times farther than the cloud heights and should be readily observable.

**Fig. 5** (PIA03452). Jupiter's northern hemisphere as viewed from a point directly over the pole. The image is a mosaic of individual images taken by the Cassini imaging system when the spacecraft was in Jupiter's equatorial plane. The pole itself was over the horizon and does not appear in these map projections. The equator is in the corners of the image



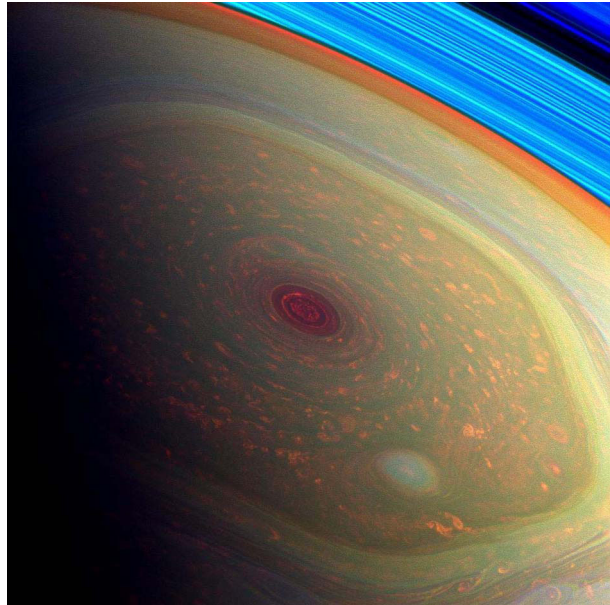
Junocam uses a filter at 889 nm to further measure cloud heights. Methane gas absorbs at this wavelength, so the photons must scatter off a high cloud if they are going to avoid absorption. Places where there are no high clouds look dark because the photons are absorbed. Photons in Junocam's other three filter bands can scatter off deeper clouds, so the high clouds do not stand out as strongly as they do in the methane band. The level of unit optical depth at 889 nm has been estimated as 540 mbar when clouds are absent (Sanchez-Lavega et al. 2013), so the methane band images will detect clouds and hazes above this level.

In principle, with multiple looks at the same place, the Junocam can measure winds. If the wind speed is  $10 \text{ m s}^{-1}$ , the cloud displacement over a 2 min time interval will be 1.2 km, which is less than the pixel size at closest approach and therefore hard to detect. But if the wind speed is  $40 \text{ m s}^{-1}$  (Vasavada et al. 1998), and if the feature stays in the field of view for 4 min—for 8 rotations of the spacecraft, then the displacement will be 9.6 km, which is measurable. The measurement will be easier if the clouds are at the same height, because then the displacement will not be confused with stereoscopic distortions due to variable cloud heights. When the spacecraft is farther away, e.g., when it is over the pole, the time that a feature is in the field of view is at most 30 min. With a  $40 \text{ m s}^{-1}$  wind, the displacement will be 72 km, which is only slightly greater than the 50 km pixel size at that point in the orbit. Nevertheless, looking for motion is worthwhile. We can rely on Earth-based instruments to measure the large-scale winds up to fairly high latitudes, but only Junocam has a chance of measuring winds at the smallest scales and at the poles.

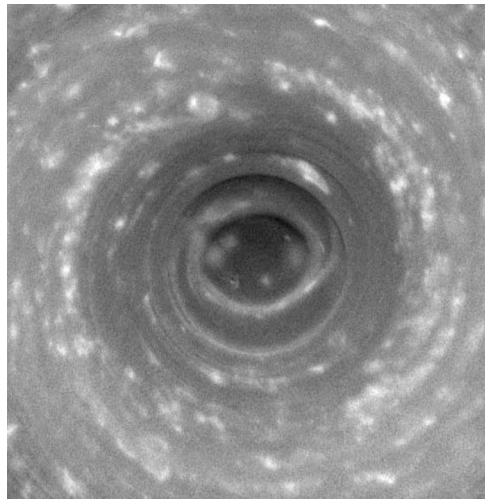
Figure 5 shows an image of Jupiter's north pole (PIA03452) that was constructed by map-projecting individual Cassini images taken as the spacecraft flew by the planet on its way to Saturn. The spacecraft was in Jupiter's equatorial plane, so the pole itself was over the horizon. Nevertheless, latitudes up to  $\sim 80^\circ$  are visible and not too badly distorted by the extreme foreshortening. The image spans from the pole to the equator in equal steps of latitude, with the zero of latitude in the corners of the image. A quadrant of this scene at higher spatial resolution (PIA03453) was made into the best-ever movie of the winds at high latitudes, but still the pole itself is invisible. The same problem exists with Voyager and Galileo, which also spent their time in the equatorial plane.

Figure 6 shows the north pole of Saturn taken by Cassini's wide-angle camera (PIA14946). The spacecraft was well above the equatorial plane, and no amount of map

**Fig. 6** (PIA14946). A portion of Saturn's northern hemisphere as viewed by Cassini from above the equatorial plane is shown. This is a single image; no map projection was necessary. The *bright blue bands* at upper right are the rings. This is a false color image with the 889 nm methane band appearing as *blue*. The *red* color (absence of *blue*) at the center indicates absence of high clouds like the eye of a hurricane. The winds are strongly cyclonic around the eye



**Fig. 7** (PIA-08332) Saturn's south pole as seen by Cassini. The edge of the image extends to  $87^\circ$  south latitude. Sunlight is coming in at the top of the image (12 o'clock position), and the eyewall clouds are casting shadows on the low clouds at the center



projection is necessary. The image shows the hexagon at  $75^\circ$  average latitude and the eye of the "Saturn hurricane" poleward of  $89^\circ$ . The colors are based on methane band imagery, with the 889 nm filter shown as blue. The reddish color of the eye (absence of blue light) indicates that the eye is a hole in the high clouds with deeper clouds underneath. The rings look blue because there is no methane gas between them and the spacecraft. Figure 7 shows a similar eye poleward of  $89^\circ$  at the south pole (PIA08332). The Sun is at the 12 o'clock position, and the shadows cast by the eyewall clouds indicate that they tower 50–70 km above the clouds within the eye (Dyudina et al. 2009). The eyewall clouds of a terrestrial hurricane top out at 15 km. The point of showing these Saturn images is that interesting

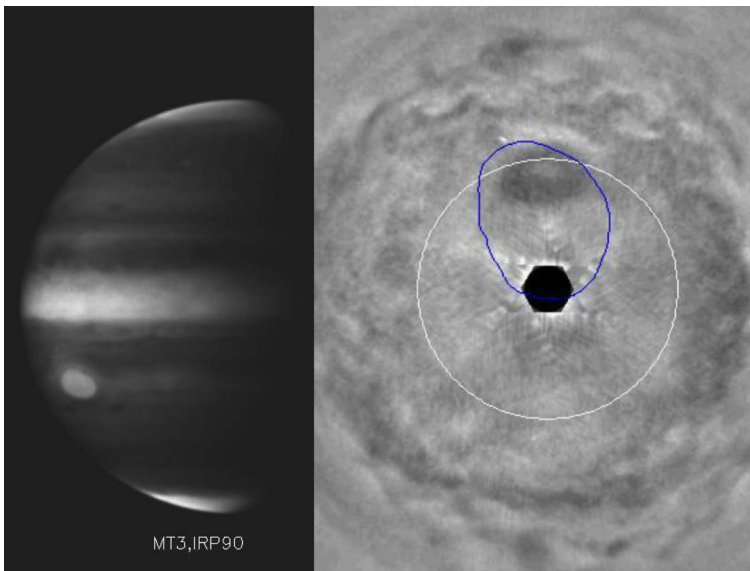


**Fig. 8** Images taken during the Cassini flyby of Jupiter showing evidence of polar clouds and haze. The *left image* (PIA02880) was taken through a filter covering the methane absorption band at 889 nm. The *right image* (PIA03473) was taken through a filter at 258 nm. It was constructed from a series of images covering all longitudes as the planet turned. The images were combined and map projected to show the north polar region as it would appear in perpetual sunlight. The pole itself is not shown because the spacecraft was in Jupiter's equatorial plane and the pole was over the horizon

things are happening at the pole of this gas giant, and we don't know if they are happening at the pole of Jupiter or not.

Figure 8 shows two images of Jupiter's north pole (PIA02880 and PIA03473). The image on the left was taken by the Cassini imaging system in the MT3 filter, which is the same as Junocam's 889 nm filter. High haze covers the polar regions, presumably because of auroral activity there. The image on the right was taken in the UV filter at 258 nm (Porco et al. 2003). This is not the same as a UV spectrum like the ones UVS will produce, but it shows the complicated wavy structure of the polar region. The image is part of an 11-day movie. The white circle is at 60° latitude, and the dark oval outlines the usual auroral zone, which is offset from the center by the tilt of Jupiter's magnetic field. As with Fig. 5, the north pole is invisible in both images because it was over the horizon as seen from the equatorial plane. The point is that the poles have special clouds and hazes that are not visible at other latitudes. These clouds and hazes show up in both UV and 889 nm images. The 889 nm filter was chosen for Junocam because it has better SNR than the 258 nm filter. Small-scale features in the polar clouds are likely to show up at 889 nm, and it is possible that they will show up in the blue filter of Junocam as well. If they do show up, they can be correlated with the lower-resolution UVS spectral images and the thermal IR images of the aurora by JIRAM.

Correlation with observations of thermal structure that will be forthcoming from ground-based support observations of polar regions will also be investigated. One of these is the detailed nature of the flow around the periphery of a broad polar vortex that is defined by a cold airmass, which appears to be coincident with the edges of a high-altitude polar haze that can be detected in the methane filter. The boundaries of both are characterized by an oscillating pattern with wavenumber 5–6. The second of these is an auroral-related heating

of the upper stratosphere by high-energy particles that likely originate with the aurora but are not close to the origin of UV or near-infrared auroral emission.

Lightning is the signature of moist convection, which is an important meteorological process and therefore of great interest to the JIRAM and MWR teams. By telling them where moist convection is occurring, Junocam will help them interpret their data. We estimate Junocam might detect one or two flashes per orbital pass. The problem is the frequency of lightning. A single storm flashes about once every 3 s (Little et al. 1999, Table III). Because they are so spread out, there are likely to be no more than several storms in a single Junocam image. The camera uses time-delayed integration to combine up to 100 exposures 3.2 ms in duration for an effective shutter time of 0.32 s. Regions on the planet are imaged 5–6 times as the spacecraft flies over them. If there are 2 or 3 storms in that region, the effective shutter time will be greater than 3 s, and the camera is likely to see a lightning flash or two during one perijove pass. The high spatial resolution is an advantage in separating lightning from cosmic rays hitting the detector. The cosmic rays light up individual pixels, whereas photons from lightning are spread out as they diffuse up through the clouds and have half-widths at half-maxima in the range 45–80 km (Little et al. 1999).

## 2.2 Jupiter's Rings

Junocam will be able to detect Jupiter's main, optically-thick ring. As the spacecraft rotates the ring will pass through the Junocam field of view. The phase angle is generally close to  $90^\circ$ , which will likely preclude detection of the more tenuous portions of the gossamer and halo rings. It will however offer the opportunity to investigate the structure and phase function of the main ring with a unique perspective from inside the rings as Juno passes through the equatorial plane.

## 2.3 Galilean Satellites

With Juno's high inclination elliptical orbit most opportunities to observe the Galilean satellites are distant and at high phase angles. Furthermore, they must be in the spin plane to be imaged by Junocam. The size and spatial scale for Junocam observations of the satellites are given in Table 1. The "optimal time to image" is within the window that the satellite is in the Junocam field of view, balancing range to the moon with lowest phase angle available.

# 3 Instrument Description

## 3.1 Overview

The Junocam instrument consists of two subsystems: the camera head (CH), which uses a build-to-print copy of the camera head electronics developed for the Mars Science Laboratory (MSL) mission with slightly modified logic and Juno-specific optics and housings, and the Juno Digital Electronics Assembly (JDEA), which contains an image buffer, power conversion circuitry, and the interface to the spacecraft. The camera head is mounted on the spacecraft's upper deck, while the JDEA is mounted to the side of the main avionics vault on the spacecraft. The two subsystems communicate via a spacecraft-provided wiring harness. Table 2 summarizes the Junocam physical characteristics.

Like previous MSSS cameras (e.g., Mars Reconnaissance Orbiter's Mars Color Imager) Junocam is a "pushframe" imager. The detector has multiple filter strips, each with a different bandpass, bonded directly to its photoactive surface. Each strip extends the entire width

**Table 1** Opportunities for Junocam observations of the Galilean satellites

Satellite	Optimal time to image	Time relative to perijove (PJ)	Subs/c latitude	Phase angle	Range (km)	Spatial scale (km/pix)	Radius (pixels)
Callisto	19 Nov 13:20	PJ4 – 50.75 h	50 N	90	244,238	159	15
Callisto	22 Dec 20:36	PJ7 – 41.5 h	57 N	61	174,732	114	21
Europa	22 March 02:52	PJ15 – 6 h	49 N	64	286,697	187	8
Ganymede	12 April 17:24	PJ17 – 24 h	47 N	61	193,244	126	21
Io	13 April 04:34	PJ17 – 13 h	48 N	62	259,344	169	11
Io	7 June 00:49	PJ22 – 3 h	48 N	58	229,462	150	12
Europa	22 July 08:58	PJ26 + 31:39	29 N	53	297,055	194	8
Europa	31 July 13:00	PJ27 – 11.5 h	9 N	100	189,837	124	12
Io	31 July 21:21	PJ27 – 3.3 h	49 N	58	193,661	126	14
Ganymede	24 Sept 08:37	PJ32 – 12.8 h	20.5 S	58	182,649	119	22
Io	24 Sept 18:02	PJ32 – 3.3 h	49 N	60	162,785	106	17

**Table 2** Junocam characteristics

Mass	2.642 kg—Camera Head 1.053 kg—JDEA
Power	4.7 W—idle 5.9 W—imaging
Dimensions	3.8 × 3.9 × 7.5 in—Camera Head 5.5 × 8.8 × 1.3 in—JDEA
Focal length	11 mm
Field of view	58 deg
Pixel size	7.4 micron
IFOV at center of field	672.7 urad

of the detector, but only a fraction of its height; Junocam's filter strips are 1600 pixels wide (spanning 58°) and about 155 rows high. The filter strips are scanned across the target by spacecraft rotation. At the nominal spin rate of 2 RPM, frames are acquired about every 400 ms. This process is illustrated in Fig. 9. At a perijove altitude of ~ 5000 km the nadir pixel, with an angular size of 0.6727 mrad, has a spatial scale of ~ 3 km. Over the pole the altitude is ~one jovian radius and the nadir spatial scale is ~ 50 km.

The spacecraft spin rate would cause more than a pixel's worth of image blurring for exposures longer than about 3.2 ms. For the illumination conditions at Jupiter such short exposures would result in unacceptably low SNR, so the camera provides Time-Delayed-Integration (TDI). TDI vertically shifts the image one row each 3.2 ms over the course of the exposure, canceling the scene motion induced by rotation. Up to about 100 TDI steps can be used for the orbital timing case while still maintaining the needed frame rate for frame-to-frame overlap.

The pushframe imaging mode requires additional processing for image reconstruction. First, each exposed frame is read out to the spacecraft and the desired bands are extracted into 128-pixel-high "framelets", editing out the unused lines between filters which may suffer from spectral crosstalk. After optional summing and compression, the framelets from all of the frames in an image are transmitted to Earth. The MSSS Ground Data System then treats each framelet as an individual image, using spacecraft attitude telemetry to map-

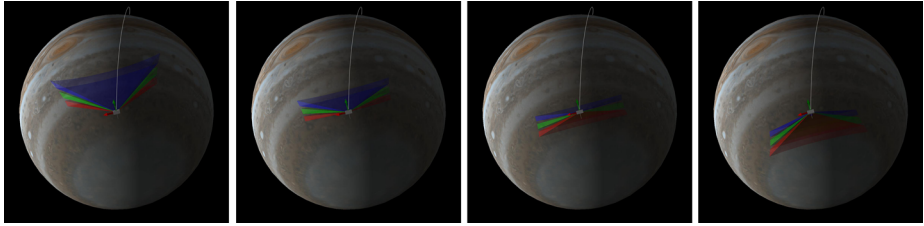
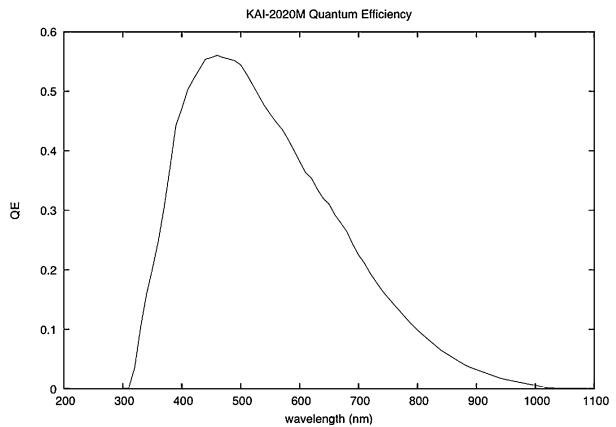


**Fig. 9** The operation of Junocam visible pushframe imaging is illustrated. Each visible band covers a  $58 \times 5$  degree field of view with its long axis parallel to the spacecraft spin axis (the *red arrow*). As the spacecraft spins, multiple frames are acquired, forming complete color coverage. Owing to the longer exposures needed, the three visible bands are acquired on one rotation, and the methane band (not shown here) is acquired on the next. The *white line* shows the north-to-south orbital path of the spacecraft

**Fig. 10** Junocam CCD quantum efficiency as a function of wavelength reaches a maximum of  $\sim 55\%$



project it onto a planetary shape model. Finally, each map-projected framelet is composited into an overall mosaic by spatial location and bandpass to form an output map.

## 3.2 Camera Head (CH)

### 3.2.1 Electronics and Detector

The CH electronics are designed around the Kodak KAI-2020 Charge-Coupled Device (CCD) image sensor. This detector has  $1640 \times 1214$  7.4-micron pixels ( $1600 \times 1200$  photoactive), and uses interline transfer to implement electronic shuttering. The sensor incorporates microlenses to improve its quantum efficiency, which peaks at about 55%. The CCD quantum efficiency as a function of wavelength is shown in Fig. 10. The “fast-dump” capability of the sensor is used to clear residual charge prior to integration and also allows vertical subframing of the final image.

The output signal from the CCD is AC-coupled and then amplified. The amplified signal is digitized to 12 bits at a maximum rate of 5 Mpixels/s. For each pixel, both reset and video levels are digitized and then subtracted in the digital domain to perform correlated double sampling (CDS), resulting in a typical 11 bits of dynamic range.

All CH functions are supervised by a single Actel RTSX field-programmable gate array (FPGA). In response to commands from the JDEA, the FPGA generates the CCD clocks,

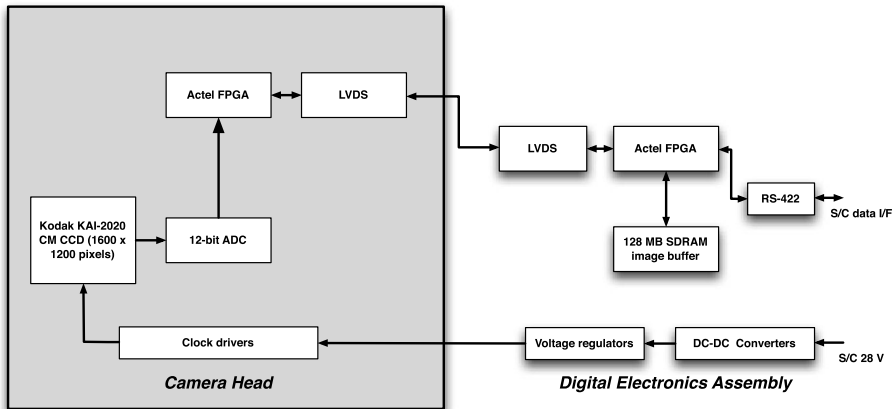


**Fig. 11** Junocam electronics functional block diagram

reads samples from the analog-to-digital converter (ADC) and performs digital CDS, and transmits the pixels to the JDEA.

The CH operates using regulated 5 V and  $\pm 15$  V power provided by the JDEA. A platinum resistance thermometer (PRT) on the camera focal plane is read by the spacecraft to provide temperature knowledge for radiometric calibration. An additional pair of PRTs and redundant etched-foil heaters are attached to the outside of the camera head and thermostatically controlled by the spacecraft.

The CH electronics are laid out as a single rigid-flex printed circuit board with three rigid sections. The sections are sandwiched between housing sections that provide mechanical support and radiation shielding, and the flexible interconnects are enclosed in metal covers. For Junocam, additional radiation shielding was required and was incorporated into the housings, which are made of titanium. An additional copper-tungsten enclosure surrounds the image sensor. The total mass of the CH is about 2.6 kg.

A functional block diagram of the Junocam electronics is shown in Fig. 11.

### 3.2.2 Filters

A color filter array with four spectral bands is bonded directly to the CCD, as shown in Fig. 12. The four bands are red (600–800 nm), green (500–600 nm), blue (420–520 nm), selected to meet SNR requirements over the pole and for ease of color reconstruction by the public, and methane (880–900 nm). The Junocam filters were fabricated by Barr Associates. The filter transmissions as measured by Barr from witness samples are shown in Fig. 13 (note that this plot also includes spectral variation of the Junocam optics). The measured center wavelengths and bandwidths are given in Table 3.

The purpose of the methane filter is to image within the narrow methane absorption band centered at 889 nm, to enhance the contrast of higher altitude clouds, as described in Sect. 2. Jupiter is quite dark in this band ( $< 5\%$  albedo) but fairly bright immediately outside it ( $> 30\%$ ). This is significant because the methane filter bandpass varies from the center to the edges of the field due to the variation in the incidence angle of the lens. An estimate of the impact of this variation is shown in Fig. 14. The dotted line shows the spectrum of

**Fig. 12** Color filters are bonded directly to the CCD

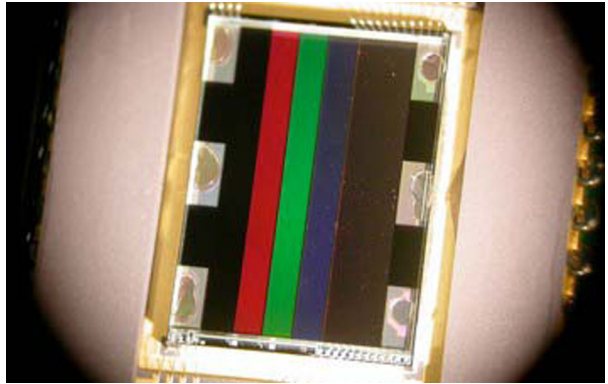


**Table 3** Junocam filter characteristics

Band	Blue	Green	Red	Methane
Center wavelength	480.1 nm	553.5 nm	698.9 nm	893.3 nm
FWHM	45.5 nm	79.3 nm	175.4 nm	22.7 nm

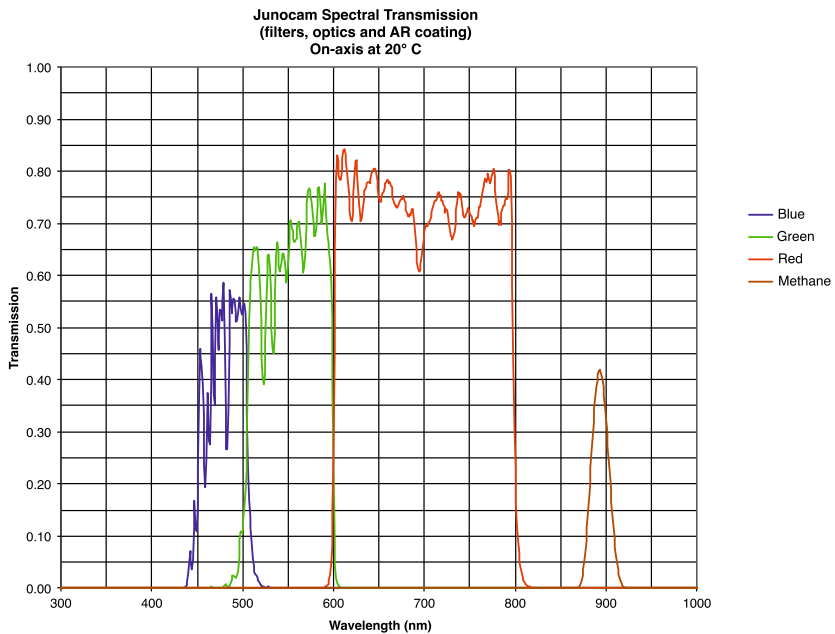


**Fig. 13** Bandpasses and transmission are shown for Junocam's four filters

Jupiter (Karkoschka 1994), with the methane absorption feature at the center. The red and blue lines show the signal as a function of wavelength for the middle of the field (red) and edges (blue). The blue line shows a 2× higher peak than the red at the shorter side of the

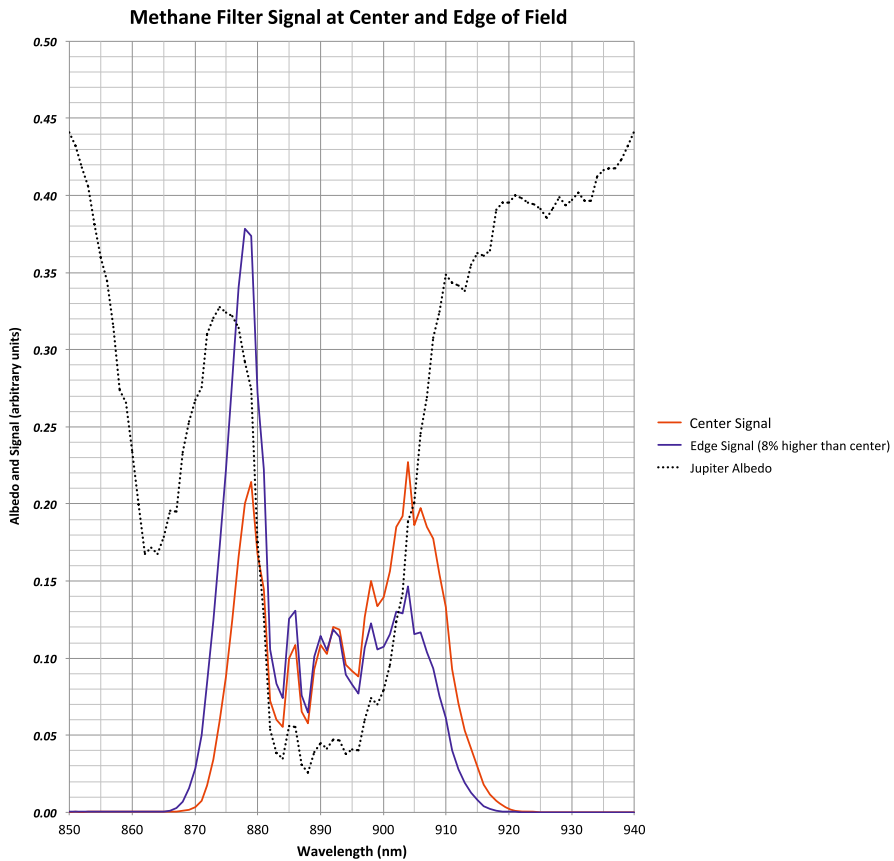


**Fig. 14** Bandpasses are shown for Junocam's methane filter with expected relative signal from the center (*red*) vs. the edges (*blue*) of the field, as described in the text. The *dotted line* shows Jupiter's albedo (Karkoschka 1994)

bandpass, and a 30 % shorter peak relative to the red on the long side. This difference yields of order 10 % more leakage (i.e., signal not from the bottom of the absorption band) at the edge of the field than at the center. It should be noted that this difference is an estimate based on the measured filter normal incidence transmission and modeled values for the off-normal transmission, and applies to both edges of the field of view.

### 3.2.3 Optics

The Junocam optics are comprised of a 14-element all-refractive lens with a nominal focal length of 11 mm and a field of view of about 58 degrees (horizontal.)  $T$ /number varies somewhat across the field and with wavelength, but the nominal on-axis  $T$ /number is 3.2. The first five front elements are made of radiation-hard glasses to provide shielding for the remaining elements, and the optics are additionally shielded by a thick titanium housing. An alignment cube is mounted to the optics to facilitate precision mounting on the spacecraft. The Junocam optics, shown in Fig. 15, were fabricated by Rockwell-Collins Optronics.

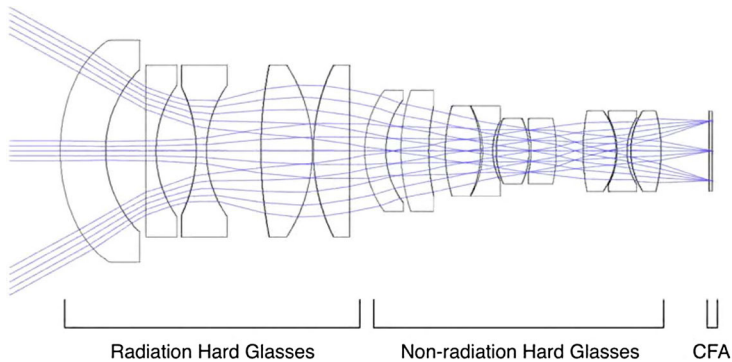


**Fig. 15** The raytrace for the Junocam optics is shown

### 3.3 Junocam Digital Electronics Assembly (JDEA)

As originally proposed, Junocam was to have used a copy of the MSL Digital Electronics Assembly (DEA), which takes raw digital image data from the camera head, compresses it in real time, and stores it in a non-volatile memory buffer for later transmission. However, it soon became apparent that the digital electronics used in the DEA (particularly its Xilinx FPGA) would likely suffer too many radiation-induced upsets from the energetic protons trapped in the jovian radiation belts. Since most of the capabilities of the DEA were unneeded for Juno, we designed a new, more radiation-resistant version, called the Junocam DEA or JDEA.

The JDEA provides regulated power to the camera head, implements a minimal command sequencing capability to manage camera head pushframe operation, receives the raw digital image data from the camera head, applies 12-to-8-bit non-linear companding, and stores the image data in a 128 MB internal DRAM buffer. The CH command/data interface is a three-signal Low Voltage Differential Signaling (LVDS) synchronous serial link transmitting commands from JDEA to CH at 2 Mbit/s and a four-signal synchronous 3-bit parallel interface from CH to JDEA at a rate of 30 Mbit/s. The JDEA also contains a command/data interface with the spacecraft, receiving higher-level imaging commands and returning image data. The command interface is a bidirectional asynchronous RS-422 interface running at 57.6 Kbaud; the data interface is a unidirectional three-signal RS-422 synchronous interface running at 20 Mbits/s.

The JDEA uses an Actel RTSX FPGA. Most of the logic design is inherited from the previously built MSSS context imager on the Mars Reconnaissance Orbiter (MRO CTX) and Lunar Reconnaissance Orbiter Camera (LROC). The power subsystem uses Interpoint components and is derived from the MSL design.

The JDEA electronics are laid out as a single rectangular printed circuit board, sandwiched between housing sections that provide mechanical support and radiation shielding. The JDEA housings are aluminum, since considerable radiation shielding is provided by the spacecraft avionics vault.

### 3.4 Flight Software

As indicated above, there is no software resident in the instrument. All additional processing is performed by software provided by Junocam and running in the spacecraft computer.

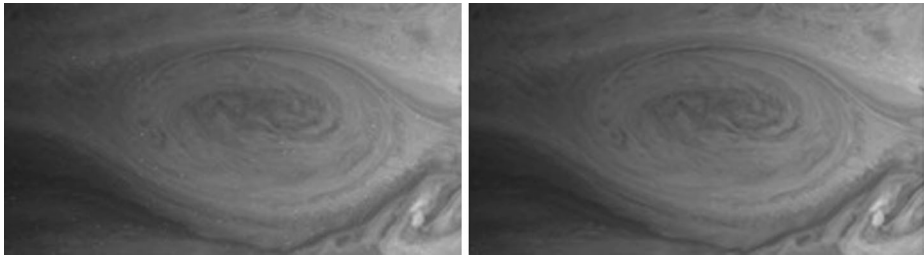


**Fig. 16** Simulated Junocam visible image showing transient effect of high particle flux, for the worst case point in the orbit (perijove +0.4 h). The left image shows simulated hot pixels from radiation. The right image is the left image after median filtering (which is done by Junocam before compression).

This software has significant commonality with that previously developed by MSSS for the Mars Odyssey and MRO missions. It is written in ANSI C and uses the VxWorks multitasking facility so that processing can occur when the spacecraft computer is otherwise unoccupied.

The software receives commands to acquire images from the spacecraft's command sequence engine. Each image command contains parameters such as exposure time, number of TDI stages, number of frames, interframe time, summing, and compression. Optionally, each image can be commanded relative to the spin phase (based on information provided by the spacecraft's attitude control system) so that only frames that are pointed at the planet need be acquired. The software instructs the JDEA to begin imaging at the appropriate time and then delays until the entire multi-frame image is acquired. It then reads out the JDEA DRAM. The raw image data are stored in spacecraft DRAM and then read out, processed, and formatted for downlinking. Processing consists of frame editing, optional summing, optional median filtering to remove radiation-induced pixel transients, and optional lossy transform-based or lossless predictive image compression.

### 3.5 Radiation Effects

There are three radiation effects likely to be observable in Junocam images. The first will be persistent hot pixels caused by displacement damage from energetic particle hits to the sensor, primarily trapped protons. Ground testing indicates that at the end of orbit 8, Junocam will have accumulated less than a hundred hot pixels, a number that can be dealt with by onboard median filter processing. There will also be a global increase in dark current, leading to a slow degradation of image quality. We estimate the dark current increase will be less than  $2\times$  through the end of orbit 8.

There will also be transient effects caused by high particle flux, effects that will vary from image to image. These effects will be localized to portions of the orbit near perijove. Because of the relatively short exposure and readout time for the visible bands ( $< 0.20$  s) and the relatively high signal levels, the impact of these transient effects are limited, and are well within the ability of the instruments median filter to remove (Fig. 16). The integration and readout time for the methane band is about twice as long as for the visible and the signal levels are more than  $10\times$  lower, making the transient radiation impact much worse (Fig. 17). Based on this analysis, the methane band will not be usable for a window less than an hour long centered at 0.4 h after perijove.

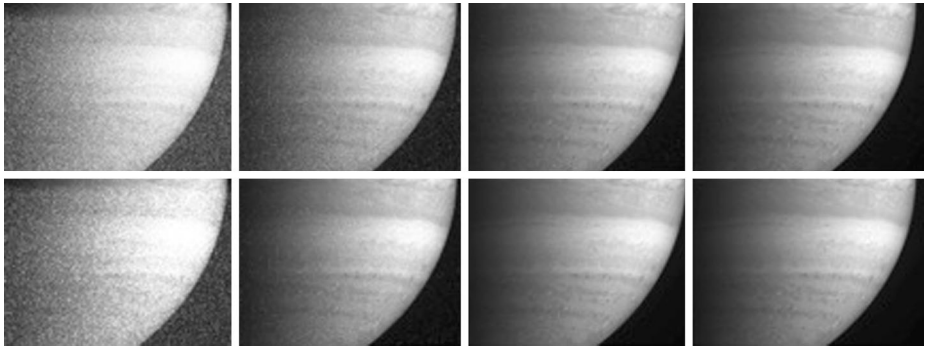


**Fig. 17** Simulated Junocam methane-band image showing transient effect of high particle flux, for points in the orbit (left to right: perijove +0.4 h, perijove +0.5 h, perijove +0.63 h and perijove -0.32 h). The upper set of images shown is without median filtering, the lower set is with median filtering. The median filter removes the transient artifacts for the -0.32 h and +0.63 h cases, but not for the +0.4 and +0.5 h cases

## 4 Calibration

Junocam was calibrated at MSSS in July 2010. Tables and figures in the following sections are the result of that calibration effort.

Calibration objectives were as follows:

- (a) *CCD Testing and Performance Validation*: Validate CCD linearity, read noise, full well, gain, bias, and dark current at system level.
- (b) *Absolute and relative radiometry*: Determine conversion between data number (DN) and radiance for each filter; measure system noise equivalent spectral radiance at each wavelength.
- (c) *Flatfields*: Determine flatfield image for each filter.
- (d) *System Spectral Throughput*: Determine relative throughput of system over each filter's bandpass; also determine rejection band throughput.
- (e) *MTF/PSF Target Imaging*: Measure Modulation Transfer Function (MTF) and Point Spread Function (PSF) at several different TDI levels.
- (f) *Geometric Mapping Function*: Determine the mapping of the angle from the optic axis in front of the lens to pixel position in the focal plane.

### 4.1 Linearity/Full Well

Linearity and full well were measured using integrating sphere images taken with a series of exposure times. This shows excellent linearity ( $r = 0.99$ ) until the full well is reached at about 1872 DN (30,500 electrons), illustrated in Fig. 18.

### 4.2 Flat Field

The instrument flat field was determined using two different techniques. In the first, the instrument imaged the exit port of the integrating sphere and was then swept in the along-row direction so that the image of the port covered the entire field of view. A composite image was then built by simply taking the maximum value of each pixel in the entire set of images. This was done for six different exposure times to provide good SNR for all spectral bands. A normalized 16-bit composite of the best exposure time for each band was

**Fig. 18** Linearity of the Junocam CCD is excellent until the full well is reached at 1872 DN/16, which occurs at 117 on this plot

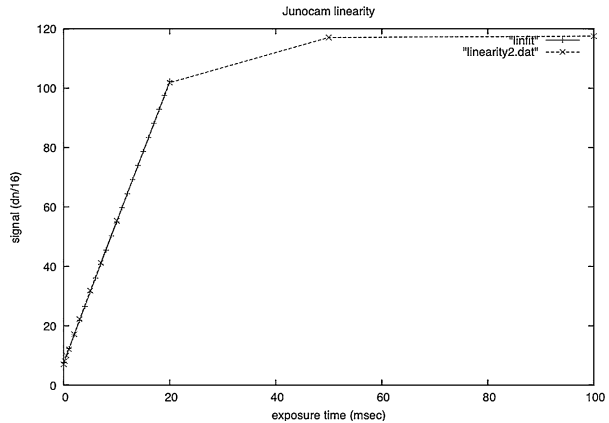
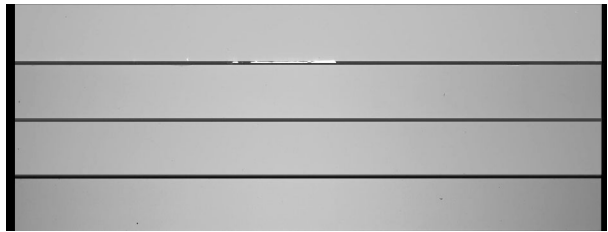


**Fig. 19** The instrument flat field is shown across the detector array. Note that this image includes the interband masked areas between the filters. These areas are edited out by the flight software for flight images



constructed and a stretched version is shown in Fig. 19. (Exposure times used were 0.5 ms for red, 1 ms for green, 5 ms for blue, and 10 ms for methane.)

#### 4.3 Dark Current and Bias

Dark current was measured in instrument thermal/vacuum tests by acquiring sets of images at different exposure times during temperature ramps. These were processed by averaging subframes with dark subtraction. The dark bias is typically a noiseless DC offset in the signal level, shown in Fig. 20. It will be removed in flight by appropriate settings of the pixel companding function (see Sect. 5).

#### 4.4 Gain and Read Noise

Based on the CCD's signal characteristics and subsequent amplification prior to digitization, the nominal system scale factor is 16.3 electrons/DN. The actual value can be expected to be slightly different due to component-to-component variation. We used the photon transfer method (Janesick et al. 1987) to measure the actual system scale factor and read noise. Different exposure times and filter band selections were used to cover a range of signal levels (Fig. 21). The scale factor derived in this manner is 15.0 e<sup>-</sup>/DN. Because the measurements were made over a limited dynamic range and were acquired in 8 bits, we recommend using the nominal scale factor, and all further analysis was done using this value.

Read noise was determined by measuring the standard deviation of dark difference images. The measured read noise was 16.6 e<sup>-</sup>.

**Fig. 20** Dark current as a function of temperature has been measured. The camera temperature at Jupiter will range between  $-26\text{ }^{\circ}\text{C}$  and  $+11\text{ }^{\circ}\text{C}$

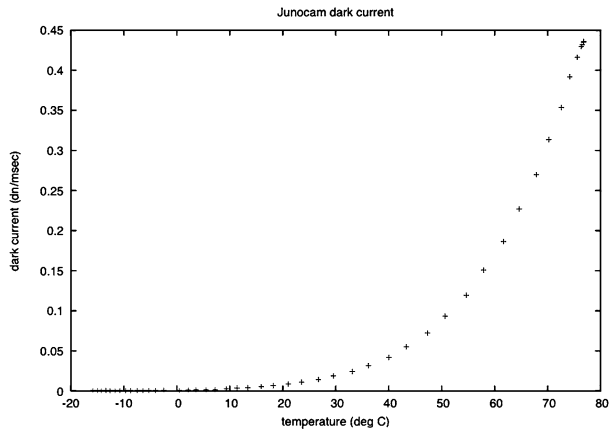
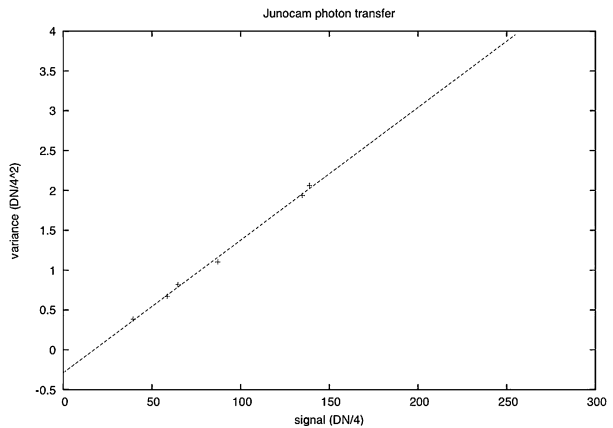


**Fig. 21** The best-fit line shows a system scale factor with divide-by-four linear companding of  $60.07\text{ e}^-/\text{DN}$  ( $r\ 0.99$ ), corresponding to a raw system scale factor of  $15.02\text{ e}^-/\text{DN}$



#### 4.5 Absolute Response

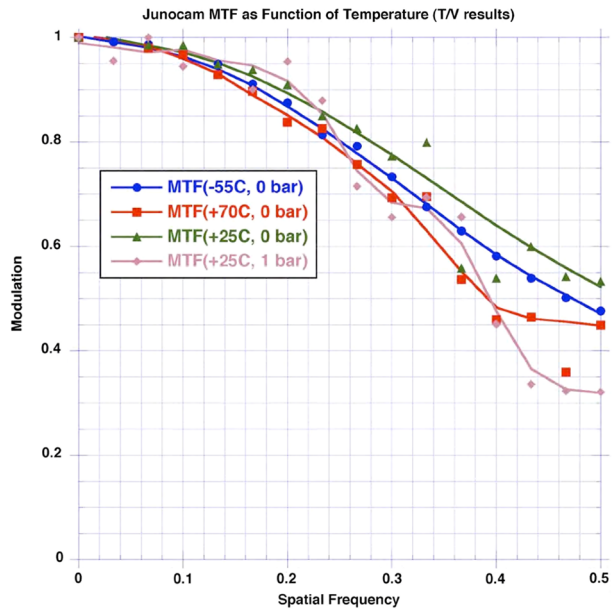
Each pixel produced by the camera is represented by a 12-bit Data Number (DN) with a scale factor of 16.3 electrons/DN. These 12-bit DNs are then converted to 8-bit form using a piecewise-linear transfer function. For normal imaging, the transfer function is set to approximate square-root encoding to preserve the full 12-bit dynamic range in the presence of shot noise. If desired, any power-of-two linear mapping can also be used (divide by 16, 8, 4, 2, or 1) to simplify data processing; any remaining high-order bits are simply discarded.

Using values for the optics and filter transmission and detector response measured during calibration, and the known solar radiance at 5.2 AU, expected signal levels are shown in Table 4. Two cases are shown: a reference case for a white lambertian target, zero incidence angle, 1 ms exposure, no TDI, and a typical Jupiter polar imaging case for a lambertian target with albedo 0.6, incidence angle 85 degrees, exposure time 3.2 ms, four TDI steps for the visible bands and 64 TDI steps for the methane band. SNR is shown for the latter case based on a measured read noise of  $17\text{ e}^-$ .

**Table 4** Junocam expected signal levels, for conditions described in the text

Band	Reference signal (e <sup>-</sup> )	Typical polar signal (e <sup>-</sup> )	Polar SNR
Red	12,669	8484	90.6
Green	10,331	6919	81.5
Blue	4766	3192	54.1
CH <sub>4</sub>	111	1191	31.0

**Fig. 22** Junocam’s Modulation Transfer Function (MTF) was measured at three temperatures during thermal/vacuum tests



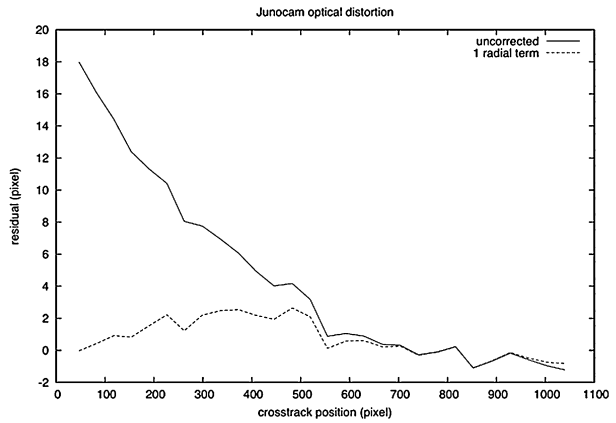
#### 4.6 Modulation Transfer Function (MTF)

The modulation transfer function, Fig. 22, was measured over temperature and pressure during instrument thermal/vacuum tests. This was done by imaging a test target through the viewport of the vacuum chamber. Note that the instrument was deliberately defocused slightly at room temperature and atmosphere, to compensate for the focus shift when going to vacuum.

#### 4.7 Geometric Calibration

The Junocam lens has low distortion (less than 3 % at the field corners, primarily barrel distortion.) Low distortion was needed so that TDI could be employed. Because of this, Junocam can be modeled to first order using a simple pinhole camera model. This can be improved by adding one radial distortion term K1, following the formulation of Brown (1966), of value 3.839251e-8. This reduces residuals across the field to less than two pixels; see Fig. 23. We expect to further refine geometric calibration using star images acquired during cruise.

**Fig. 23** Residuals between actual pixel measurements of a dot target and camera models are shown. The *solid line* uses the function for an ideal pinhole lens; the *dashed line* uses a model incorporating a radial distortion



#### 4.8 Stray Light

Our primary concern regarding stray light was the potential for visible light to leak under the narrowband methane filter. We measured this using the integrating sphere and the Quartz-Tungsten-Halogen (QTH) lamp, with and without an 850 mm long-wave-pass filter in place between the lamp and the sphere input. The signal level in the methane band was about 88 DN without the filter and about 74.3 DN with it, a leakage of about 18.4 %, but there was little evidence of structure in the leakage, so this is mostly leakage in the filter bandpass itself. Stray light from bright sources just outside the field shows no more than 1–2 % of additional signal.

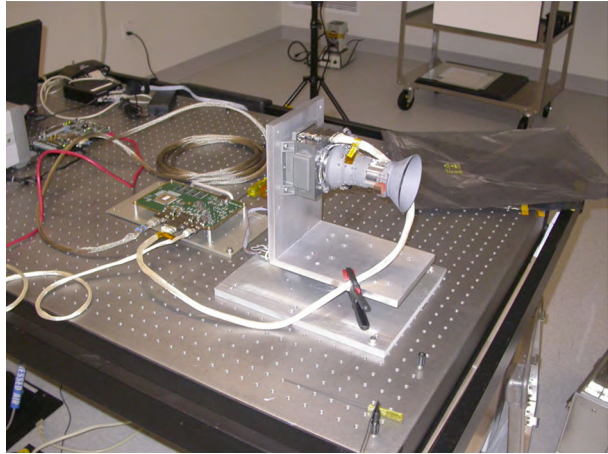
Mounted on the spacecraft, the off-sun angle must be greater than  $75^\circ$  to avoid direct illumination of the front lens element by rays not blocked by the sunshade. Ordinarily the spacecraft is oriented such that the solar arrays face the sun, which puts the sun at an angle of  $90^\circ$  from the boresight, so scattered light is not an issue.

#### 4.9 Alignment

The camera head is mounted to the spacecraft using an L-shaped bracket provided by the spacecraft vendor. The camera pointing can be precisely controlled by the use of adjustable shims at the bracket mounting interface. Typically, wide field-of-view systems do not have stringent alignment requirements, but since Junocam uses TDI, its CCD had to be precisely aligned to the spacecraft spin axis so that scene motion is exactly along CCD columns. A precision reflective alignment cube was provided on the optics to control alignment. Prior to instrument delivery, the angle between the cube normal and the CCD columns was measured. This was accomplished by taking a sequence of images of a long straight target that had been leveled relative to gravity while rotating the camera about its boresight and taking successive images. Once the target was aligned with the CCD rows, the camera was rotated again until a direct return to a laser level from the alignment cube face was observed. This angle was provided to the spacecraft vendor for use in alignment during mounting.

Post-mounting alignment verification was then performed by directly imaging a test target with Junocam. The position of each dot on the target was surveyed photogrammetrically in the spacecraft coordinate system, and the image of each dot on the camera focal plane determined by thresholding and centroiding the image. The dot locations in space were then

**Fig. 24** Junocam was mounted on a motorized rotation stage for TDI tests



mapped back to focal plane position using a camera model. Analysis of the dot positions shows that the spin axis is within 2 milliradians of the CCD column axis, well under the maximum requirement of 7.8 milliradians imposed by one column of crosstrack drift in 128 TDI steps.

#### 4.10 TDI Polarity

It is critically important for TDI that the direction be correct—if for example a sign error anywhere in the chain results in TDI going in the opposite sense of the spacecraft rotation all advantage to building up SNR will be lost and images will be hopelessly smeared. For end-to-end TDI polarity verification, we mounted the camera on a National Aperture Inc MM-4M-R motorized rotation stage, shown in Fig. 24, and drove it at the nominal spacecraft rate of 2 RPM. Motion was restricted to a 90-degree arc for cable management reasons.

Figure 25 shows the results of this test, which verified that the direction of the TDI was as desired to be consistent with the direction of spacecraft rotation.

#### 4.11 Cruise Imaging

Imaging of the receding Earth-Moon system, taken on 26 August 2011 (about 21 days after launch) at a distance of about 9.7 million kilometers, shown in Fig. 26, provided the first verification that Junocam was functional after launch. The images validated that the electronics and optics were all performing as expected.

Subsequent inflight checkouts have validated the tests done before launch, and provide the additional reassurance that the mounting on the spacecraft and coordinate conversions were all done properly. Figure 27 shows a test image taken on 14 March 2012 of several familiar star fields; these images were taken in the red band with 80 TDI steps. The center of this image (not shown) was saturated with scattered sunlight. Given Junocam's sunshade geometry, the off-sun angle must be  $> 75^\circ$  to avoid scattered light.

Junocam imaged the Earth and Moon again during the Earth flyby in October 2013. Results are discussed in Sect. 6.4.

**Fig. 25** This color image mosaic was taken with TDI = 4 while Junocam was moving at the nominal rate of 2 RPM. Residual color artifacts are from uncorrected parallax effects and sensor blooming from direct imaging of the overhead lights. This image would have been blurred if TDI had been implemented incorrectly

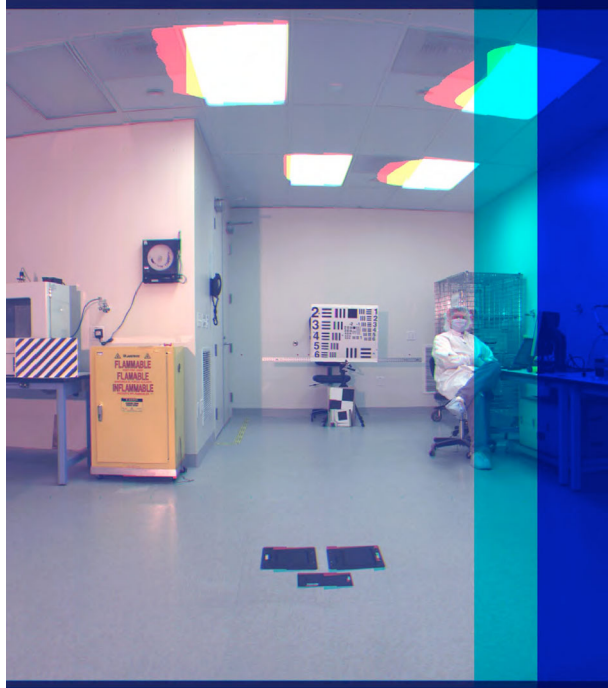
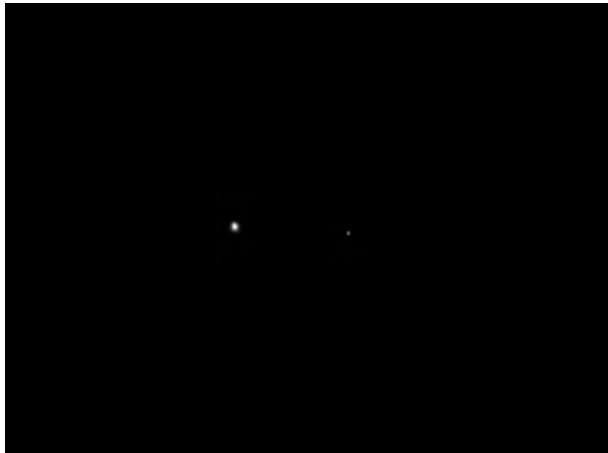


**Fig. 26** Junocam imaged the earth and the moon a few weeks after launch, on 26 August 2011, 6 million miles (9.66 million km) away

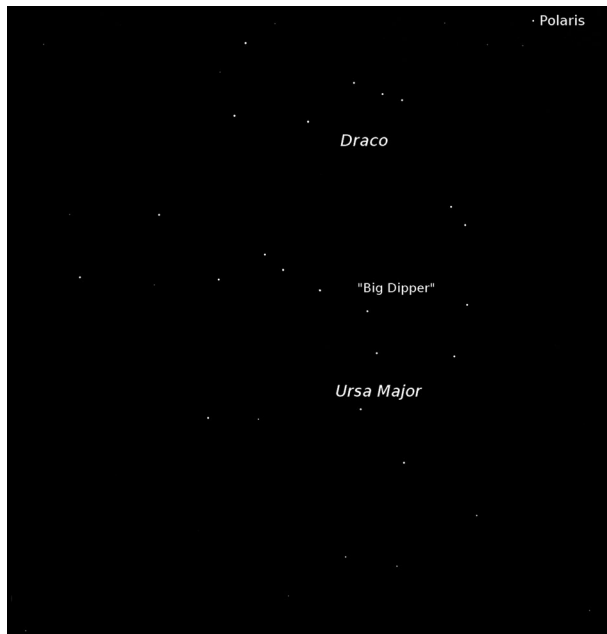


## 5 Operations and Commanding

### 5.1 Image Acquisition

Eight parameters need to be set to acquire an image: the number of TDI stages, per-frame exposure time, compression level, companding, color bands to be acquired, number of frames to be taken, interframe times, and summing (0 for red, green and blue filters or  $2\times$  for methane). Although companding (going from 12 bits to 8 bits) can be specified, in general the default (square root) will be used.

**Fig. 27** Images of star fields acquired in cruise validate the orientation and mounting of the camera. This image of a familiar star field was acquired on 14 March 2012



Because the methane filter requires  $2\times$  summing to reach an acceptable SNR, the methane image will be acquired in a separate rotation from the red-green-blue images. It is possible to take individual red, green and blue images if desired, but normally all 3 will be acquired in the same spacecraft rotation.

The interframe (time between frames) is in units of milliseconds. The maximum value is 65 s. When the interframe time is set to zero, the software computes an appropriate value based on the spin rate as provided by the spacecraft's attitude control system. (In this case the commanded exposure time is ignored and the actual exposure time is computed based on the spin rate and the commanded TDI.)

Compression choices are: no compression, lossless predictive compression, or lossy Discrete Cosine Transform (DCT)-based compression with selectable requantization. Larger requantization values yield more compression at the cost of diminished image quality. Ground simulations show that we can expect a high level of compression without significant impact to image quality early in the mission, before radiation damage has accumulated, as shown in Fig. 28. The onboard median filtering should correct for most effects of radiation damage to image quality.

## 5.2 Orbital Timeline

Figure 29 shows a portion of Juno's highly elliptical polar orbit. In general Junocam will be off for most of the orbit although there will be exceptions, for example to take Galilean satellite images, or acquire a time-lapse movie. Typically the camera will be powered on several hours prior to perijove, then powered off again several hours after perijove.

At the beginning of the prime mission the spacecraft is almost directly over the north pole at  $\sim 1$  h before perijove and over the south pole at  $\sim 1$  h after perijove. Most imaging will be done in a two-hour period centered at perijove. For planning purposes, we split this period

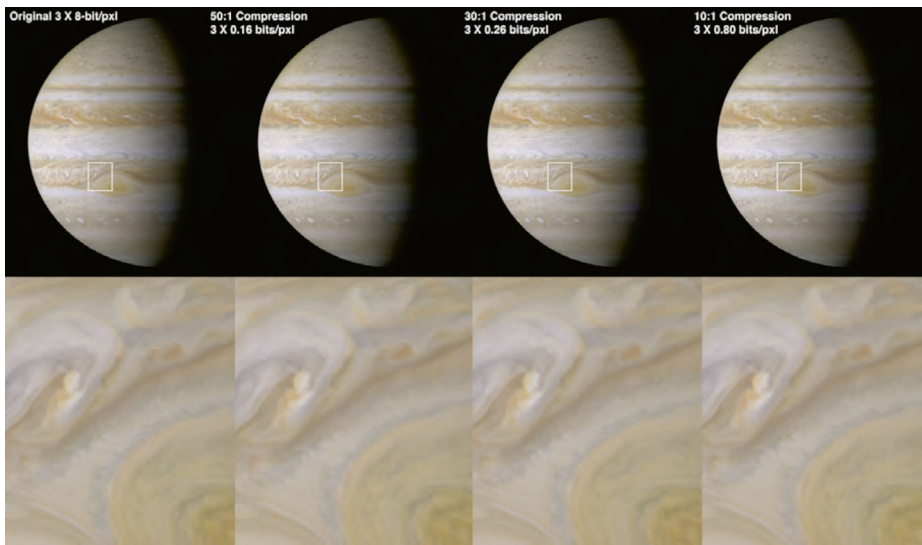
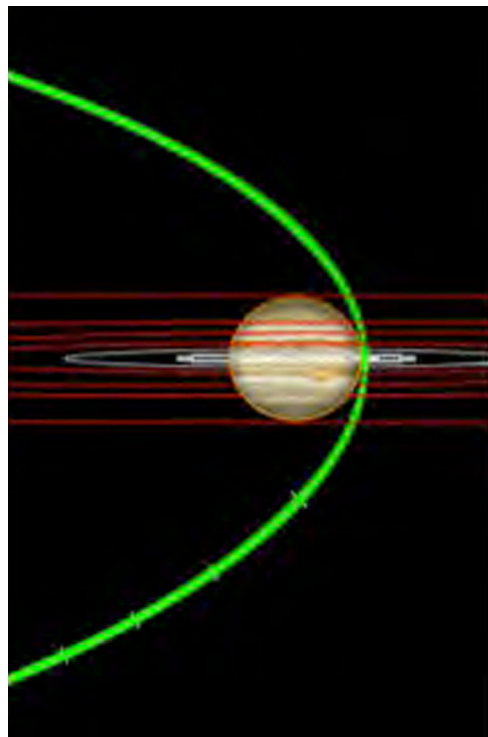


**Fig. 28** Different levels (labeled) of simulated image compression are shown. As radiation damage accumulates the commanded level of compression will be adjusted

**Fig. 29** Approximately 1 day of Juno's 11-day elliptical polar orbit is shown. The orbit will pass inside Jupiter's ring and intense radiation belts



into 120 discrete imaging opportunities; with the nominal spacecraft spin rate of 2 rpm, a 4-color image can be acquired once per minute. Because of limited downlink data volume and

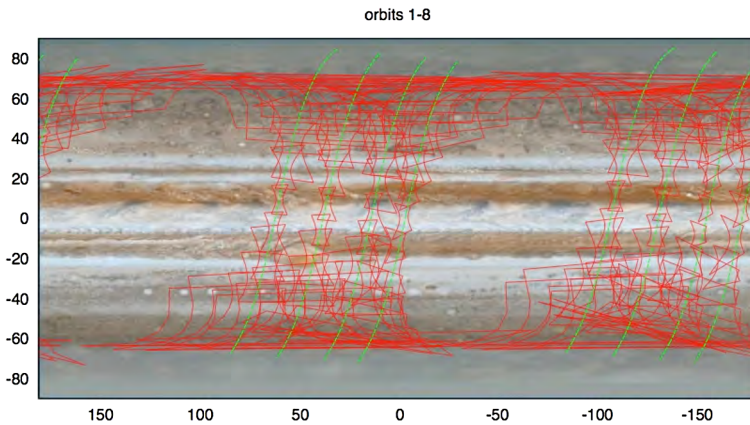


**Fig. 30** Junocam footprints are outlined in *red* for the first 8 orbits. The *green lines* show the spacecraft nadir track for one orbit. The coverage from a single spacecraft rotation forms a “bowtie” on the planet with its narrowest part at the nadir and its widest at the visible limbs; the total size of the bowtie increases with increasing spacecraft altitude. On this simple cylindrical projection, the complete coverage of the poles is not shown

other camera readout limitations, not all of these images can be taken, so the main purpose of the planning process is to select which are most desirable, balanced against the amount of compression.

Figure 30 shows that with judicious choices Junocam images can be acquired from pole to pole in a contiguous swath. With just 8 orbits (the required lifetime of the camera) mid- and equatorial latitudes will not be completely covered.

Because of Juno's eccentric orbit, Jupiter's size decreases rapidly as Juno moves away from perijove, as shown in Fig. 31. This means that time-lapse movies will not obtain global coverage at very good resolution. Even so, for outreach purposes we hope to acquire one movie around an entire orbit early in the mission. The rapid changes in scale and perspective guarantee a dramatic sequence, as shown in Fig. 4.

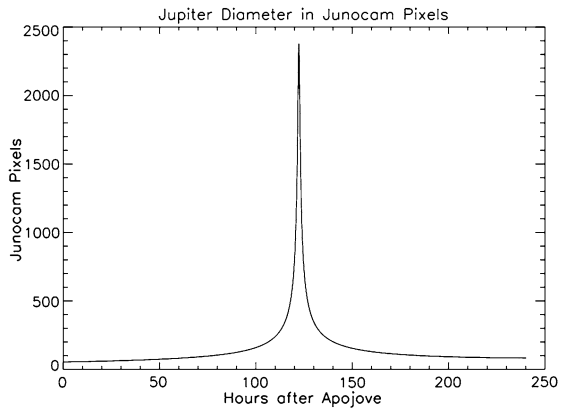
### 5.3 Stereo Imaging

At its maximum velocity near periapsis, it takes about 7 min for the subspacecraft point to reach the visible limb. This means that images acquired less than 7 min apart will contain overlap regions seen at different viewing angles, allowing fore-aft stereo imaging. This may permit photogrammetric determination of the vertical structure of the cloudtops, though radiation transients near periapsis could complicate processing. A 4-color image can be obtained once per minute; at the minimum altitude of 4300 km, Juno's speed is  $57 \text{ km s}^{-1}$ , which means Junocam could image a point on the planet at emission angles of  $0^\circ$ ,  $\pm 38^\circ$ ,  $\pm 67^\circ$ , etc. At higher altitudes and slower velocities the number of possible emission angles is greater and the difference between them is less, so one might want to take images less frequently than once per minute.

### 5.4 Image Data Volume

Junocam image data is stored in dedicated framed partition space in the spacecraft computer. This limits the number of images that can be collected during the hours around per-

**Fig. 31** The size of Jupiter in pixels over one orbit is shown. The combination of Juno's elliptical orbit and the wide angle optics of Junocam result in high resolution images being achievable only in the hours surrounding perijove. A dramatic zoom movie will be acquired in Orbit 2



ijove when the spacecraft is not returning telemetry in real-time. The Junocam partition is 1181 Mb.

The size of a Junocam image varies depending on the size of Jupiter in the field of view and the type of compression selected. An uncompressed 4-color image requires  $\sim 75$  Mb at the moment in time  $\sim 1$  h from closest approach that Junocam resolution is better than Cassini. About 15 min later Jupiter fills the Junocam field of view and a 4-color uncompressed image with direct view of the pole requires  $\sim 100$  Mb. At perijove a 4-color uncompressed image requires  $\sim 120$  Mb. Very roughly that means that  $\sim 10$  uncompressed images could be stored in a perijove pass. With compression the number will be substantially higher. We expect to achieve at least a factor of 2 compression, and likely much higher than that at the beginning of the prime mission when accumulated radiation damage is minimal.

## 6 Outreach Plans

In keeping with the outreach goals for Junocam, we intend to open up our operations so that the world can see how planetary science on a spacecraft is carried out. The general outreach theme for Junocam is “science in a fishbowl”. We will provide insight into the scientific planning process and the factors that influence scientific decisions. As the images are processed and analyzed, the link will be made between science planning and outcomes. The Junocam concept for operations relies on public involvement at three stages: advance planning, image selection, and image processing, as described in the following sections. Although some of the details may change, the inclusion of the public in the operation of Junocam drives our decision-making. With a very small professional operations team, and together with the professional community involved in active observations of Jupiter, we are relying on the public to fill in key pieces of Junocam operation. The public is an essential part of our virtual team.

### 6.1 Advanced Planning and the Amateur Astronomy Community

Jupiter's dynamic atmosphere presents an ever-changing pattern of reddish-brown belts and white zones. In order to anticipate what a given image of Jupiter will look like it is necessary to have current, not historic, images. We will rely on the amateur community, as well as the professional community such as those associated with the International Outer Planet Watch, to supply their most up-to-date ground-based pictures.

A web portal will be provided for images from the amateur astronomy community to be posted and organized. The location of some stable features in Jupiter's dynamic atmosphere such as the Great Red Spot can be predicted well in advance. For others, predictions from the community will be made based on the available data in 2016. [Due to the solar conjunction in September 2016, ground-based observations of Jupiter will not be possible at the beginning of the Juno science mission and will likely not resume for several science orbits. In this timeframe we will rely on predictions from pre-conjunction ground-based images and Junocam images taken in Juno's capture orbit.]

Based on amateur inputs and early images from Junocam, simulations of possible Junocam image footprints for each upcoming orbit will be posted on the web, for use in image selection.

## 6.2 Image Selection and Execution

Data volume constraints will typically limit the total number of images in a perijove pass to  $\sim 15$ . Image targets must be selected roughly two weeks in advance of their acquisition for incorporation into the final spacecraft command sequence. Selection factors include:

- Juno orbital location, resolution, and lighting geometry;
- What features of interest are visible;
- The degree of radiation effects from both transient effects (which vary with spacecraft latitude) and accumulated damage.

Graduate students will participate in the image selection process. Based on simulations of the series of images for the two hours around periapsis, students will write blog entries promoting specific images, based on science rationales and other factors. A comment system, open to the public, will be provided to encourage a dialog about the merits of particular observations.

The public will be invited to help prioritize image candidates. The prioritized list will be used by the Junocam operations team will use to create camera commands. The public list will be merged with other requests from the Juno science team, and as many images as possible will be acquired until onboard memory dedicated to Junocam images is exhausted. The web portal will provide access to the planning, dialogs, prioritized list, and the final image products, organized by science orbit.

## 6.3 Downlink and Data Processing

Initial image processing will be carried out at MSSS to construct the most basic image products. There are three types of products: (1) Experiment Data Records (EDRs) in decompressed image framelet order, 8 bits/pixel, as received from the spacecraft; (2) Reduced Data Records (RDRs) in decompressed flat-fielded form, framelet order, 16 bits/pixel; and (3) map-projected images. The data will then be made available via the web. Our goal is to have the images published within days of their receipt on the ground.

For additional products, we will rely on the image data processing amateur community. While basic processing will be done by image processing professionals, we will primarily be encouraging the general public to be creative. Some possible areas of effort are feature tracking, visualizations using other Juno instrument data and/or ground-based observations, methane mapping, and false color. We will encourage the public to provide figure captions and describe their processing techniques. This portion of our outreach plan was tested at the earth flyby.

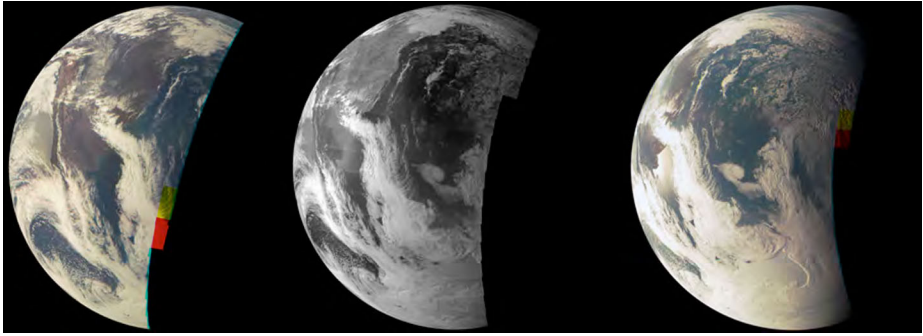


**Fig. 32** These three JunoCam images of Earth were taken on 3 separate spacecraft rotations. The *leftmost image* was taken at 19:08 UT at a altitude of 5741 km; the *center image* was taken at 19:11, 4001 km, and the *rightmost image* at 19:12, 3197 km. The *center image* was taken using JunoCam's narrowband methane filter; the other two are combinations of the instrument's *red, green, and blue* filters and approximate natural color. Each image is a mosaic of 82 individual frames taken as the spacecraft spun; these have been composited and remapped by ground processing

The web portal will be used to highlight these public contributions. When stereo is available we will encourage the making of visualization products like flyovers. The web portal will also have links to other publicly available papers and reports with scientific analysis of the content of the images.

#### 6.4 The 2013 Earth Flyby

The Juno spacecraft flew by earth on October 9, 2013 for a gravity assist on its way to Jupiter (Bolton et al. 2014). JunoCam was powered on for  $\sim 10$  min to take pictures of the moon and for about an hour to take pictures of the earth. A total of 17 images were acquired, including the moon, Jupiter, the dayside of the earth mostly over South America, the nightside of the earth over Africa, and a few test images. We had several goals for the earth flyby:

1. Acquire JunoCam images of an extended object to validate expected camera performance and test image reconstruction tools
2. Test map projection software on an extended object using the JunoCam-specific camera model
3. Provide data to the amateur image processing community and encourage them to produce a variety of products

Figure 32 shows a series of images acquired as the spacecraft passed over the dayside of the earth, which validate the first and second goals. These were processed at MSSS and illustrate that the image build, map projection and color reconstruction tools perform as planned. The first shows the southern two-thirds of South America. As the spacecraft moves eastward, the Chilean coast and the snowy line of the Andes mountains recedes toward the limb. The third image has a good view of the Argentinean coastline with specular highlights off the Rio Negro north of Golfo San Matias, as well as cloud formations over the continent of Antarctica.

In order to achieve the third goal images were posted on the MSSS website within minutes after receipt at MSSS. Different stages of processing were available to the public—raw framelets, map-projected images, and preliminary color versions. A tutorial was provided.

The amateur community responded with many beautiful and creative products. A sample of these are highlighted on the NASA Juno website: [www.nasa.gov/mission\\_pages/juno/multimedia/](http://www.nasa.gov/mission_pages/juno/multimedia/) with a more complete collection posted on [missionjuno.swri.edu](http://missionjuno.swri.edu).

**Acknowledgements** At MSSS, Junocam was designed and built by Jake Schaffner, Paul Otjens, Chris Martin, Hakeem Oluwo and Mike Malin. Operations support is provided by Robert Zimdar and Elsa Jensen. The Junocam optics were developed by Rockwell Collins Optronics, an effort supported by Chris Yarbrough, Charlie Micka, David Wallis and John Fitzpatrick. The team expresses its appreciation to the Juno spacecraft team at Lockheed-Martin Space Systems, especially Jeanne Ladewig, Jennifer Delavan, Valerie Rowland, and Chuck Rasbach. At the Juno Project at JPL our thanks go to Amy Snyder Hale, Mark Boyles, Phil Morton, Tim Koch, Randy Dodge, Michela Muñoz Fernández, Steven Watson and Steve Matousek. Junocam was developed for NASA under contract 1287931 with the Jet Propulsion Laboratory, California Institute of Technology.

**Open Access** This article is distributed under the terms of the Creative Commons Attribution License which permits any use, distribution, and reproduction in any medium, provided the original author(s) and the source are credited.

## References

- A. Adriani et al., Space Sci. Rev. JIRAM, The Jovian Infrared Auroral Mapper (2014, this issue)
- S.K. Atreya, Atmospheric moons Galileo would have loved, in *Galileo's Medicean Moons—Their Impact on 400 Years of Discovery*, ed. by C. Barbieri et al.. IAU Symp. P Series, vol. 269 (Cambridge University Press, Cambridge, 2010), pp. 130–140
- G.L. Bjoraker, H.P. Larson, V.G. Kunde, The abundance and distribution of water-vapor in Jupiter atmosphere. *Astrophys. J.* **311**, 1058–1072 (1986)
- S. Bolton et al., Space Sci. Rev. The Juno Mission (2014, this issue). doi:[10.1007/s11214-014-0040-z](https://doi.org/10.1007/s11214-014-0040-z)
- D.C. Brown, Decentering distortion of lenses. *Photogramm. Eng.* **32**(3), 444–462 (1966)
- U.A. Dyudina, A.P. Ingersoll, S.P. Ewald, A.R. Vasavada, R.A. West, I.H. Baines, T.W. Momary, A.D. Del Genio, J.M. Barbara, C.C. Porco, R.K. Achterberge, F.M. Flasar, A.A. Simon-Miller, L.N. Fletcher, Saturn's South polar vortex compared to other large vortices in the Solar System. *Icarus* **202**, 240–248 (2009)
- K.S. Edgett, R.A. Yingst, M.A. Ravine, M.A. Caplinger, J.N. Maki, F.T. Ghaemi, J. Schaffner, J.F. Bell, L.J. Edwards, K.E. Herkenhoff, E. Heydari, L.C. Kah, M.T. Lemmon, M.E. Minitti, T.S. Olson, T.J. Parker, S.K. Rowland, J. Schieber, R.J. Sullivan, D.Y. Sumner, P.C. Thomas, E.H. Jensen, J.J. Simmonds, A.J. Sengstacken, R.G. Willson, W. Goetz, Curiosity's Mars Hand Lens imager (MAHLI) Investigation. *Space Sci. Rev.* **170**, 259–317 (2012)
- P.J. Gierasch, A.P. Ingersoll, D. Banfield, S.P. Ewald, P. Helfenstein, A. Simon-Miller, A. Vasavada, H.H. Breneman, D.A. Senke, G.I. Team, Observation of moist convection in Jupiter's atmosphere. *Nature* **403**, 628–630 (2000)
- R. Gladstone et al., Space Sci. Rev. The Ultraviolet Spectrograph on NASA's Juno Mission (2014, this issue)
- J.R. Janesick, K.P. Klaasen, T. Elliott, Charge-coupled-device charge-collection efficiency and the photon-transfer technique. *Opt. Eng.* **26**(10), 260972 (1987). doi:[10.1117/12.7974183](https://doi.org/10.1117/12.7974183)
- M. Janssen et al., Space Sci. Rev. MWR: Microwave Radiometer for the Juno Mission to Jupiter (2014, this issue)
- E. Karkoschka, Spectrophotometry of the Jovian planets and Titan at 300- to 1000-nm wavelength: the methane spectrum. *Icarus* **111**, 174–192 (1994)
- B. Little, C.D. Anger, A.P. Ingersoll, A.R. Vasavada, D.A. Senke, H.H. Breneman, W.J. Borucki, Galileo ISS Team, Galileo images of lightning on Jupiter. *Icarus* **142**, 306–323 (1999)
- P.R. Mahaffy, H.B. Niemann, A. Alpert, S.K. Atreya, J. Demick, T.M. Donahue, D.N. Harpold, T.C. Owen, Noble gas abundance and isotope ratios in the atmosphere of Jupiter from the Galileo Probe Mass Spectrometer. *J. Geophys. Res., Planets* **105**, 15061–15071 (2000)
- H.B. Niemann, S.K. Atreya, G.R. Carignan, T.M. Donahue, J.A. Haberman, D.N. Harpold, R.E. Hartle, D.M. Hunten, W.T. Kasprzak, P.R. Mahaffy, T.C. Owen, N.W. Spencer, Chemical composition measurements of the atmosphere of Jupiter with the Galileo Probe mass spectrometer. *Adv. Space Res.* **21**, 1455–1461 (1998)
- J.L. Ortiz, G.S. Orton, A.J. Friedson, S.T. Stewart, B.M. Fisher, J.R. Spencer, Evolution and persistence of 5- $\mu$ m hot spots at the Galileo probe entry latitude. *J. Geophys. Res., Planets* **103**, 23051–23069 (1998)

- C.C. Porco, R.A. West, A. McEwen, A.D. Del Genio, A.P. Ingersoll, P. Thomas, S. Squyres, L. Dones, C.D. Murray, T.V. Johnson, J.A. Burns, A. Brahic, G. Neukum, J. Veverka, J.M. Barbara, T. Denk, M. Evans, J.J. Ferrier, P. Geissler, P. Helfenstein, T. Roatsch, H. Throop, M. Tiscareno, A.R. Vasavada, Cassini imaging of Jupiter's atmosphere, satellites, and rings. *Science* **299**, 1541–1547 (2003)
- M. Roos-Serote, S.K. Atreya, M.K. Wong, P. Drossart, On the water abundance in the atmosphere of Jupiter. *Planet. Space Sci.* **52**, 397–414 (2004)
- A. Sanchez-Lavega, J. Legarreta, E. Garcia-Melendo, R. Hueso, S. Perez-Hoyos, J.M. Gomez-Forellad, L.N. Fletcher, G.S. Orton, A. Simon-Miller, N. Chanover, P. Irwin, P. Tanga, M. Ceconi, Colors of Jupiter's large anticyclones and the interaction of a tropical Red Oval with the Great Red Spot in 2008. *J. Geophys. Res., Planets* **118**, 2537–2557 (2013)
- M.A. Uman, *The Lightning Discharge* (Academic Press, New York, 1987)
- A.R. Vasavada, A.P. Ingersoll, D. Banfield, M. Bell, P.J. Gierasch, M.J.S. Belton, G.S. Orton, K.P. Klaasen, E. DeJong, H.H. Breneman, T.J. Jones, J.M. Kaufman, K.P. Magee, D.A. Senske, Galileo imaging of Jupiter's atmosphere: The Great Red Spot, equatorial region, and White Ovals. *Icarus* **135**, 265–275 (1998)